Slope stability and rock fall hazard assessment of volcanic tuffs using RPAS with 2D FEM slope modelling

Ákos Török[1], Árpád Barsi[2], Gyula Bögöly[1], Tamás Lovas[2], Árpád Somogyi[2], and Péter Görög[1]

[1]Department of Engineering Geology and Geotechnics, Budapest University of Technology and Economics, Budapest, H-1111, Hungary
[2]Department of Photogrammetry and Geoinformatics, Budapest University of Technology and Economics, Budapest, H-1111, Hungary

Correspondence to: Ákos Török (torokakos@mail.bme.hu)

Abstract. Low strength rhyolite tuff forms steep, hardly accessible cliffs in NE Hungary. The slope is affected by rock falls. RPAS (Remotely Piloted Aircraft System) was used to generate a digital terrain model (DTM) for slope stability analysis and rock fall hazard assessment. Cross sections and joint system data was obtained from DTM. Joint and discontinuity system was also verified by field measurements. On site and laboratory tests provided additional engineering geological data for modelling. Stability of cliffs and rock fall hazard were assessed by 2D FEM (Finite Element Method). Global analyses of cross-sections show that weak intercalating tuff layers may serve as potential slip surfaces, however at present the highest hazard is related to planar failure along ENE-WSW joints and to wedge failure. The paper demonstrates that without RPAS no reliable terrain model could be made and it also emphasizes the efficiency of RPAS in rock fall hazard assessment in comparison with other remote sensing techniques such as terrestrial laser scanning (TLS) and tachymetry.

1 Introduction

In the past years, technological development of RPAS revolutionized the data gathering of landslide affected areas (Rau et al. 2011), recultivated mines (Haas et al. 2016), monitoring coastal processes (Casella et al. 2016), levee breaches (Brauneck et al. 2016) or road cuts (Mateos et al. 2016). RPAS has been increasingly used in engineering geology; historical landslide mapping (Jovančević et al. 2016) and in slope stability analyses (Niethammer et al. 2012, Fraštia et al 2014,) RPAS can be combined with terrestrial laser scanning (TLS) since both remote sensing tools provide high precision terrain measurement (Fanti et al. 2013, Assali et al. 2014, Francioni et al. 2014, Neugrig et al. 2016, Manconi & Giordan 2015). These tools can be used to validate height information derived by other technologies. Rock falls represent special landslide hazards since their rapid movements and various trajectories make it difficult to predict their hazard potential (Crosta & Agliardi 2003, Manconi & Giordan 2014). Several methods have been suggested to assess cliff stability from physical prediction rock fall hazard index (Crosta & Agliardi 2003) via Rockfall Hazard Rating System (Budetta 2004) and modelling of their trajectories (Crosta & Agliardi 2002, Abbruzzese et al. 2009, Copons et al. 2009, Samodra et al. 2016). These methods rely on understanding failure mechanisms and on predicting displacement of rock masses (Pappalardo et al. 2014, Stead & Wolter 2015, Mateos et al. 2016) or at some cases individual rock blocks (Martino & Mazzanti 2014). To gather data on the rock fall hazard of existing cliff faces, a number of crucial data is needed: slope profiles, material properties, block size (De Biagi et al. 2017) and possible discontinuity surfaces that can contribute to slope instability. Slope profiles can be obtained from point clouds, while material properties have to be measured on site (e.g. Uniaxial Compressive Strenght by Schmidt hammer) or under laboratory conditions (Margottini et al. 2015). Detection and mapping of joints require fieldwork (on site measuring by compass), or at hardly accessible locations it is possible by applying remote sensing techniques (Fanti et al. 2013), or both.

Most of rock fall hazard publications deal with hard, well cemented rocks such as limestone (Samodra et al. 2016) or various other types of sedimentary rocks (Michoud et al. 2012), igneous or metamorphic rocks. In contrast, very few previous studies

deal with cliff face stability and rock fall hazard of low strength rock such as volcanic tuffs (Fanti et al. 2013, Margottini et al. 2015). Volcanic tuffs are very porous rocks and prone to weathering (Arikan et al. 2007). While the current paper deals with a low strength pyroclastic rock, it has a slightly different approach of cliff stability analysis, since slope stability is assessed by using a combination of remote sensing techniques, field measurements, and laboratory testing of tuffs with 2D FEM (Finite Element Analysis) analyses of slopes. Compared to other case studies this study operates on a smaller scale and studies the possibilities of wedge and planar failures. The cliff face is unstable as it is evidenced by falling blocks. Due to rock fall hazard, the small touristic pathway was closed to avoid causalities. The current paper analyses the cliff faces by condition assessment and stability calculations. Thus, this research provides an assessment of how RPAS can be used to create a surface model at hardly accessible sites. The paper also demonstrates the combined use of photogrammetric, surveying, and engineering geological methods at difficult ground conditions in assessing rock slope stability.

2 Study area

The study area is located at mid mountain range in NE-Hungary. A hardly accessible jointed rhyolite tuff cliff face was studied. On the top of the cliff a touristic point, the Sirok Castle is located (Fig. 1). The steep rhyolite tuff hill with an elevation of 298 m and found at the transition area of two mountain ranges, Mátra and Bükk Mountains. The tuff is very porous and prone to weathering (Török et al. 2007).
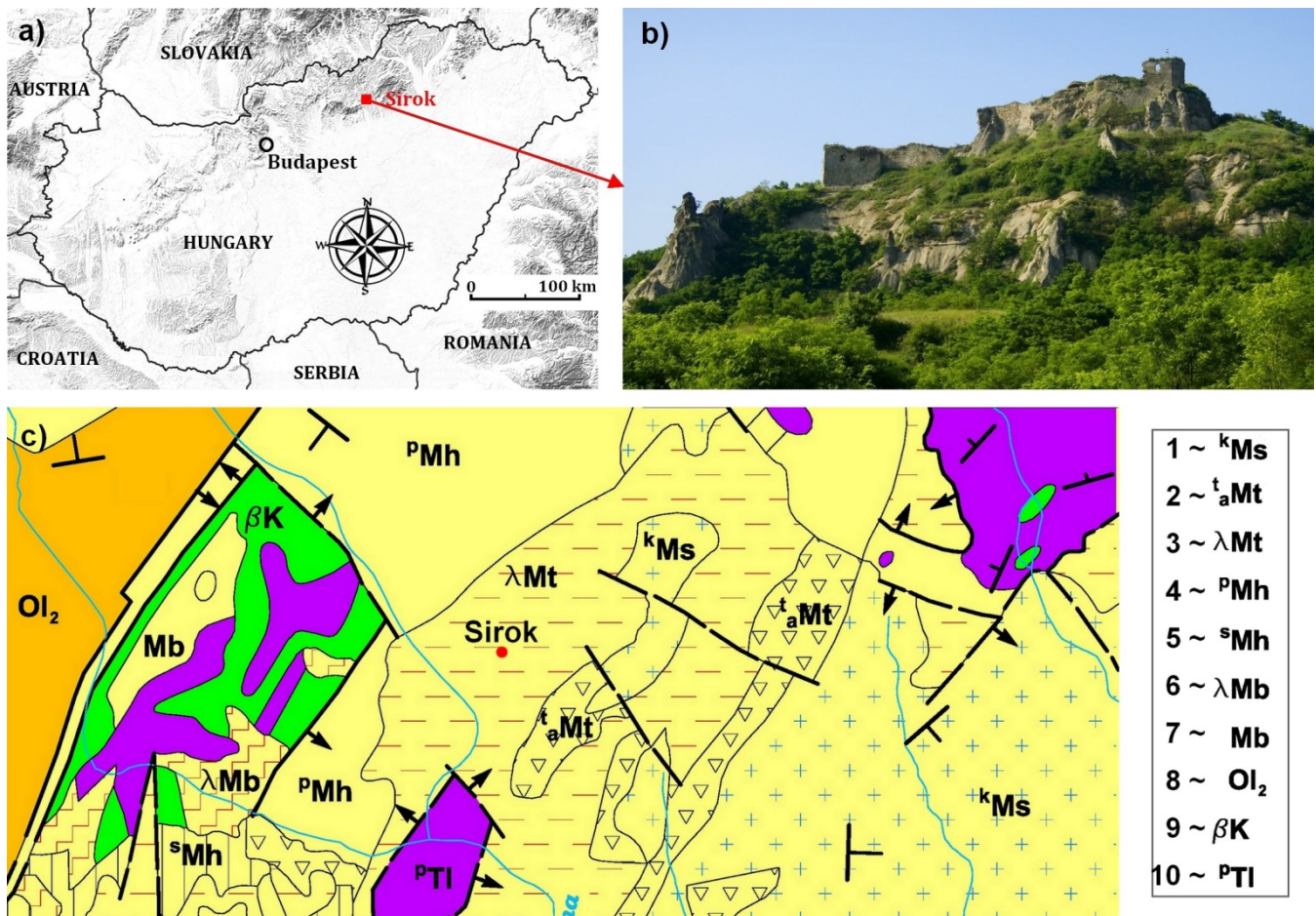
Fig.1. Location of studied cliff faces and an image of the rocky slope at Sirok Castle, NE Hungary (top) and the geological map of the area (redrawn after Balogh 1964) (bottom). Legend for geological map: Miocene (1-7), Oligocene (8), Cretaceous (9), Triassic (10): 1: gravel and conglomerate; 2: clay; 3:rhyolite tuff; 4: sand and sandstone; 5: siltstone; 6: rhyodacite tuff; 7: fine sand; 8: clay; 9: basalt; 10: radiolarite.

Although the first castle was already constructed in the 13th century AD, due to war damages and reconstructions, the current structure encompasses wall sections representing different construction periods. In these days, the partially ruined walls have been restored, and the castle is open to tourists but southern slopes are closed due to rock fall hazard.

The hill represents a rhyolite tuff that was formed during the Miocene volcanism (Badenian-Lower Pannonian period). The cliff face was formed during to the late Miocene volcanic activity. It is a part of the Inner Carpathian volcanic chain. The geological map of the closer area clearly reflects the dominance of pyroclastic rocks, with isolated occurrences of Oligocene and Triassic rocks (Fig. 1). The cliffs are steep and display several joints and discontinuity surfaces. The present study focuses on the southern hillslope of the castle hill, where major rock falls occurred in the near past (Fig. 2). The study area is divided into smaller units, where RPAS and rock fall hazard assessment analyses were carried out (Fig 3).

Fig.2. Studied southern cliff faces (clockwise): a) image of the castle obtained by RPAS with marked details; b) distant view of the eastern part of the cliff section; c) weathered rounded cliff with larger taffoni; d) vertical to sub-vertical cliff face with steep joints and traces of rock fall; e) steep cliffs dissected by joints.

Fig.3. Location of the illustrations in the paper and the sections (1 to5 marked by yellow dashed lines) where slope stability was calculated by using 2D FEM model (Fig.8). Dotted lines indicate the areas shown on Fig. 4 and Fig. 7.

3 Materials and Methods

5 The research contains two major methods: i) RPAS and ii) engineering geology. The applied methods are summarized in a flow diagram displaying the combination and links between (Fig. 4). The explanation of these research methods are given below in more details.
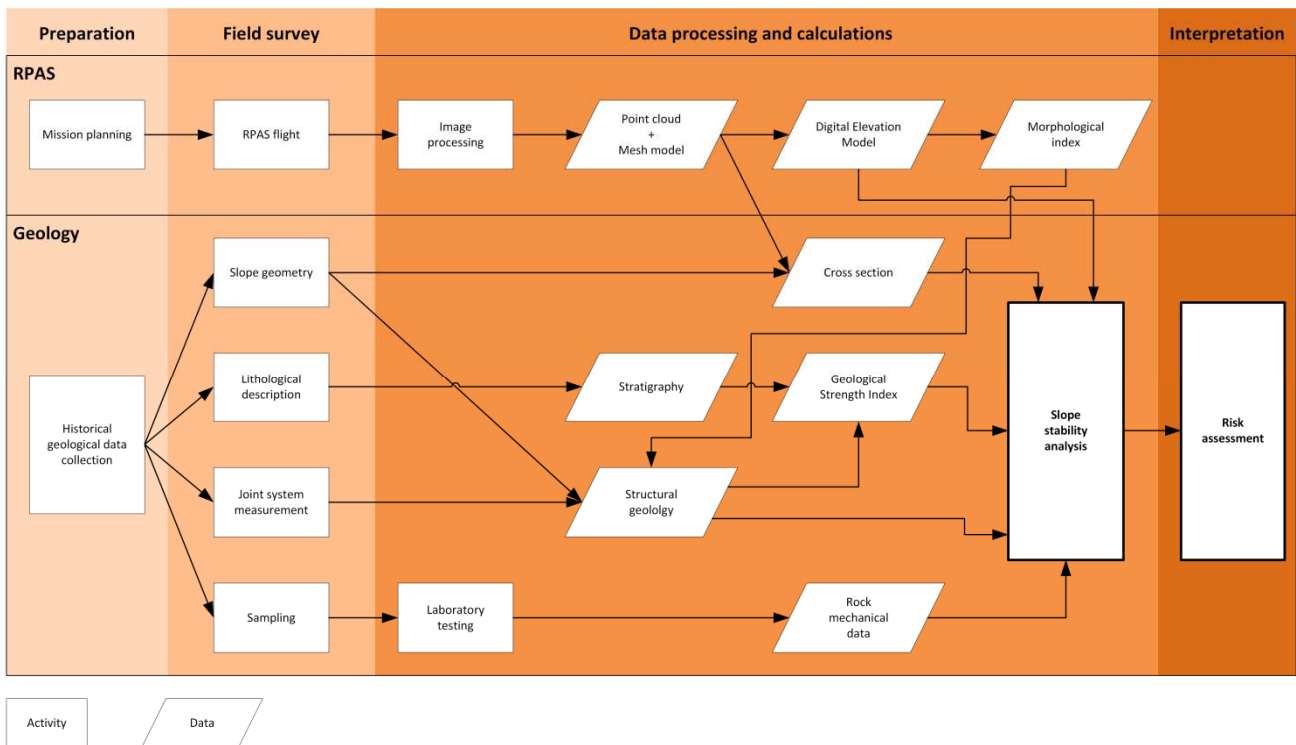
10 **Fig.4. Flow chart showing the methods and obtained data set of this paper indicating the interrelationship between RPAS, geological analyses and risk assessment (see details in the text)**

3.1 RPAS data acquisition and terrain modelling

For cliff stability analysis a digital terrain model was required. It assumes the accurate 3D modelling of the highly dissected rock faces. Since major parts of the site consist of hardly accessible steep slopes that are partly covered by vegetation, traditional surveying was not possible. As a consequence, RPAS technology was applied (Fig. 4). By the use of RPAS, high amount of images was captured, and then a 3D point cloud was generated to enable surface modelling. The point cloud was validated by terrestrial laser scanning, which is a mature, widely used technology in creating detailed, accurate surface models.

The Remotely Piloted Aerial System (RPAS) was deployed on 21st February 2015, when vegetation cover was limited. The system is a modified commercial DJI Phantom 2 drone (DJI, 2016), where the flying vehicle has been equipped with a synchronous image transfer that also forwards the current flying parameters (e.g. height, speed, tilt, power reserve). Due to the complexity of the survey area, the flight was controlled manually; the required overlap between images was ensured by the operator considering capture frequency. For safety reasons, the crew consisted of two persons: one for controlling the aircraft, the other one for continuously monitoring the transferred video stream. The camera control is done by a tablet.

A GoPro Hero 3+ (GoPro, 2017) action camera was mounted onto a 2-DoF gimbal of the unmanned aerial vehicle (UAV). The camera has a fixed 2.77 mm focal length objective that is capable of capturing 4000 × 3000 pixel sized JPG images. The images were captured with a sensitivity of ISO 100 and sRGB color space. The lens was used with a fixed aperture of 2.8 and the camera was able to adjust the adequate shutter speed. Generally the exposure time was set to 1/1400 s and the images were compressed at a rate of 4.5 bits/pixel. There were three imaging flights; two around noon and one about 5 in the afternoon. The flying times were 13, 12 and 13 minutes, respectively, where 390, 365 and 419 images were captured. All 1174 images were involved in the photogrammetric object reconstruction (Fig. 5). The photogrammetric reconstruction has been done by Pix4Dmapper (Pix4D, 2017), which is based on Structure-from-Motion (SfM) technology (Westoby et al. 2012, Danzi et al. 2013, Lowe 2004). SfM automatically identifies tie points considering initial requirements (e.g. preliminary image centre positions, time stamps). Camera calibration was executed during post-processing, no prior calibration was needed. After the image alignment, the image projection centres and attitudes can be observed in (Fig. 4). 12 million points were obtained by the photogrammetric reconstruction.
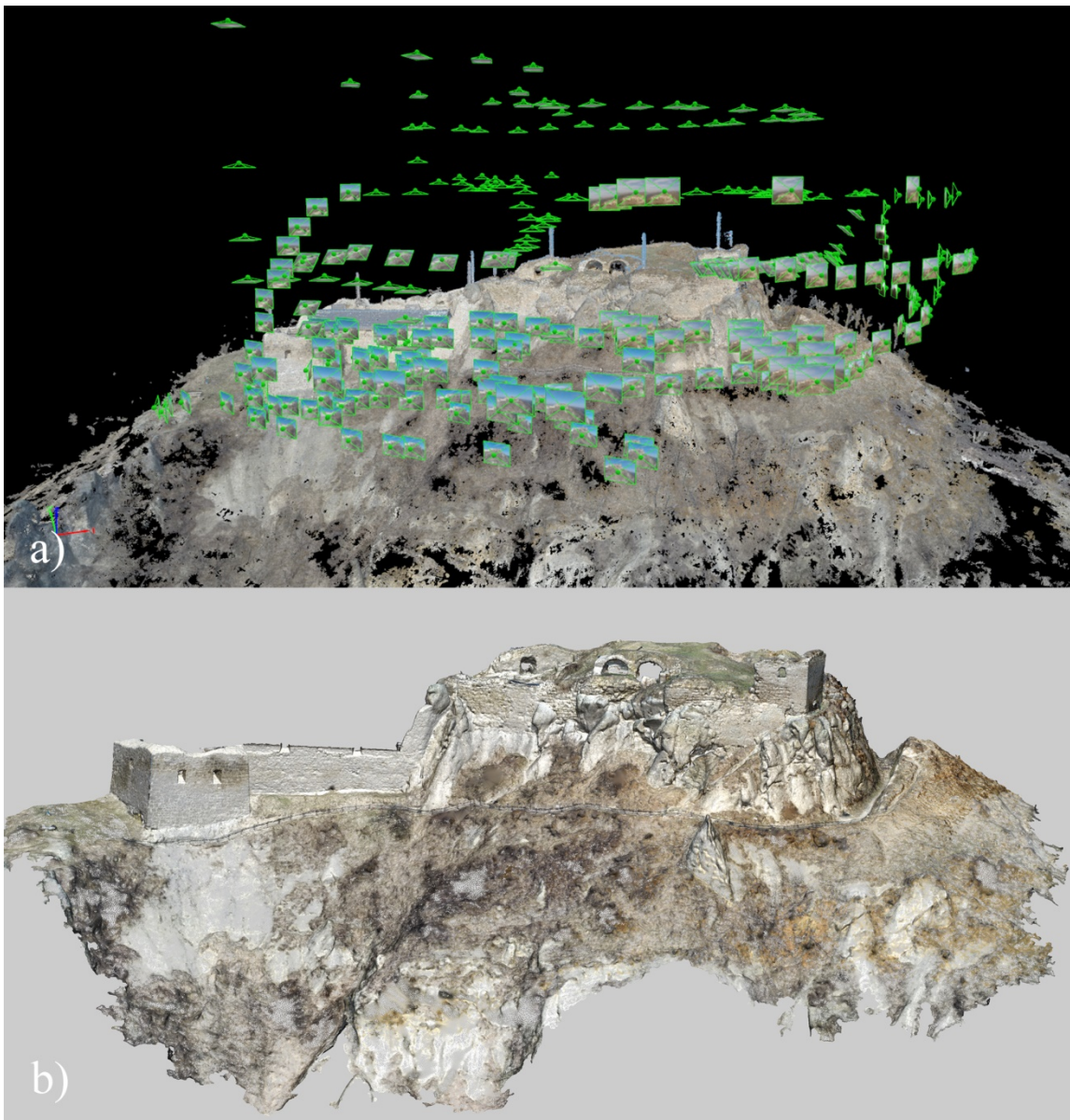
Fig.5. The captured image positions around the reconstructed castle hill (top) and the point clouds obtained by RPAS technology (bottom) (see top view on Fig. 3.)

Due to georeferencing, particular tie objects had to be measured also by Global Navigation Satellite System (GNSS). The used GNSS receiver was a Leica CS10 with a Gs08plus antenna (GS08, 2014, CS10, 2014). The measurement was done in RTK mode supported by the Hungarian RTK network (RTKnet, 2013). There were 7 measured ground control points (GCPs); the mean 3D measurement accuracy was 4.9 cm (minimal value was 2 cm, maximal value 9 cm).

10   The RPAS data collection was validated by the use of terrestrial laser scanning. The necessary data were captured by two scanners, a Faro Focus S 120 3D (Faro, 2016) and a Z+F Imager 5010C (Z+F 2014). The terrestrial laser scanning was executed on the same day as the RPAS mission. The raw point cloud measured by Faro scanner contained 1.9 billion points, whilst the Z+F point cloud 0.8 billion points. Both point clouds have X, Y Z coordinates, intensity and RGB color values. RPAS and TLS based point clouds could be compared by the software CloudCompare (CloudCompare, 2014) (Fig. 4).

15   The RPAS technology has produced considerable amount of points. Since this point cloud is difficult to be managed due to its size, and heterogeneous point spacing, the later processing requires a sophisticated resampling step, which was done by CloudCompare, where the spatial resolution of the point cloud was set to 1 cm.

The point cloud was then imported into Geomagic Studio 2013 (GeomagicStudio, 2013) and meshed, where the triangle side length was 5-7 cm (Fig. 7). To support the geological survey, several horizontal and vertical sections were derived in Geomagic DesignX 2016 (GeomagicDesignX, 2016); these profiles were exported in CAD-format (Fig. 5).

The next step was to make cut-offs focusing only on the cliffs; it was done by CloudCompare, followed by the points being exported in LAS-format (LAS, 2012). The exported points could then be imported into SAGA GIS 2.1.2 (Conrad et al. 2015), where the necessary DEMs were created by inverse distance weighting (IDW) algorithm (IDW, 2013). The derived DEM-grids have 5 cm spatial resolution, which is adequate for morphologic analyses (Fig. 4). The morphology analysis has concentrated on Catchment Area (CA) (Haas et al. 2016), although several other morphological indices (e.g. Topographic Wetness Index, Stream Power Index) were derived (Fig. 4). These indices express the potential relationship between surface geometry and geological parameters.

3.2 Engineering geology and slope stability analysis

Major lithotypes were identified and described and geological profiles were recorded during the engineering geological field surveys (Fig. 4). Rock joints, discontinuity surfaces and fault systems were measured by using compass and structural geological software applied in mobile phone. The structural geological data was analysed by Dips software. Strength parameters were assessed on site by using a Schmidt hammer. 10 rebound values were measured on each surface and mean values and standard deviations were also calculated. This method has been also used previously to gather rapid data on rock strength of cliff faces (Margottini et al. 2015). The data-set was compared to rock mechanical laboratory tests.

Samples for laboratory analyses were collected on site (Fig. 4). Major rock mechanical parameters were measured under laboratory conditions on cylindrical specimens. These were drilled from blocks and cut into by appropriate size using cutting disc. The sizes of tested specimen were made according to EN on air dry and on water saturated samples. The specimens were grouped according to the bulk density and the propagation speed of the ultrasonic pulse wave. Strength parameters such as uniaxial compressive strength, an indirect tensile strength (Brasilian), was measured according to relevant EN standards and ISRM suggested methods and modulus of elasticity was also calculated (Table 1). The generalized Hoek-Brown failure criterion (Hoek et al. 2002) was used to determine strength parameters of the rock mass. Altogether, 53 cylindrical test specimens were used for the tests.

Table 1. Rock mechanical tests and relevant standards.

Rock mechanical parameter	Number of specimens	Relevant standard
Bulk density	53	EN 1936:2000
Water absorption	18	EN 13755:2008
Propagation speed of the ultrasonic wave	53	EN 14579:2005
Uniaxial compressive strength	31	ISRM 2015
Modulus of elasticity	31	ISRM 2015
Tensile strength (Brasilian)	23	ISRM 2015

The falling blocks can endanger the touristic footpath bellow the castle on the southern slopes, therefore the stability analysis of the rocky slopes was focused on this part of the cliff (Fig. 3). First, the rock mass failure was analysed with by the RocFall FEM software of the Rocscience (RS2). The steepest sections were determined from to the terrain model obtained from RPAS data. The GSI values of the rock masses were determined according to Marinos et al. (2005). The global stability of the hillslope of selected sections was calculated with RS2 software. Since the rhyolite tuff is a weak rock with few joints the rock mass failure and the failure along discontinuities were also analysed. This kinematic analysis had been done with stereographic tool. The orientations of main joint sets were obtained from RPAS (DTM model, Fig. 4) and at accessible

areas were also measured on site on the southern and south-eastern parts of the hillslope. Additional measurements were also made in the underground cellar system of the castle, where the tuff is also exposed. The Dips software was used for the kinematic analysis. The direction of the hillslopes and the direction of the discontinuities were compared to determine the location of the potential hazardous failure zones on the hillside. Stereographic plots were generated showing the possible

5   failure planes for all slope directions and the safety factor of the possible planar failure was calculated by Rocplane software. Wedge failure was modelled by Swedge software. Toppling failure due to geological and geomorphological conditions cannot occur. Risk assessment was based on slope stability calculations (Fig. 4).

4. Results

The rhyolite tuff faces consist of moderately bedded ignimbritic horizons and also brecciated lapilli tuffs and tuffs according

10   to our field observations (Fig. 6). The topmost 10 metres of the cliff face which was modelled from slope stability comprises 3 main horizons and can be modelled as "sandwich structure". The lower and the upper part are formed by thick pumice containing lapilli tuffs. These beds enclose nearly 2 metres of well-bedded less-welded fine tuff and brecciated horizons (Fig. 6).
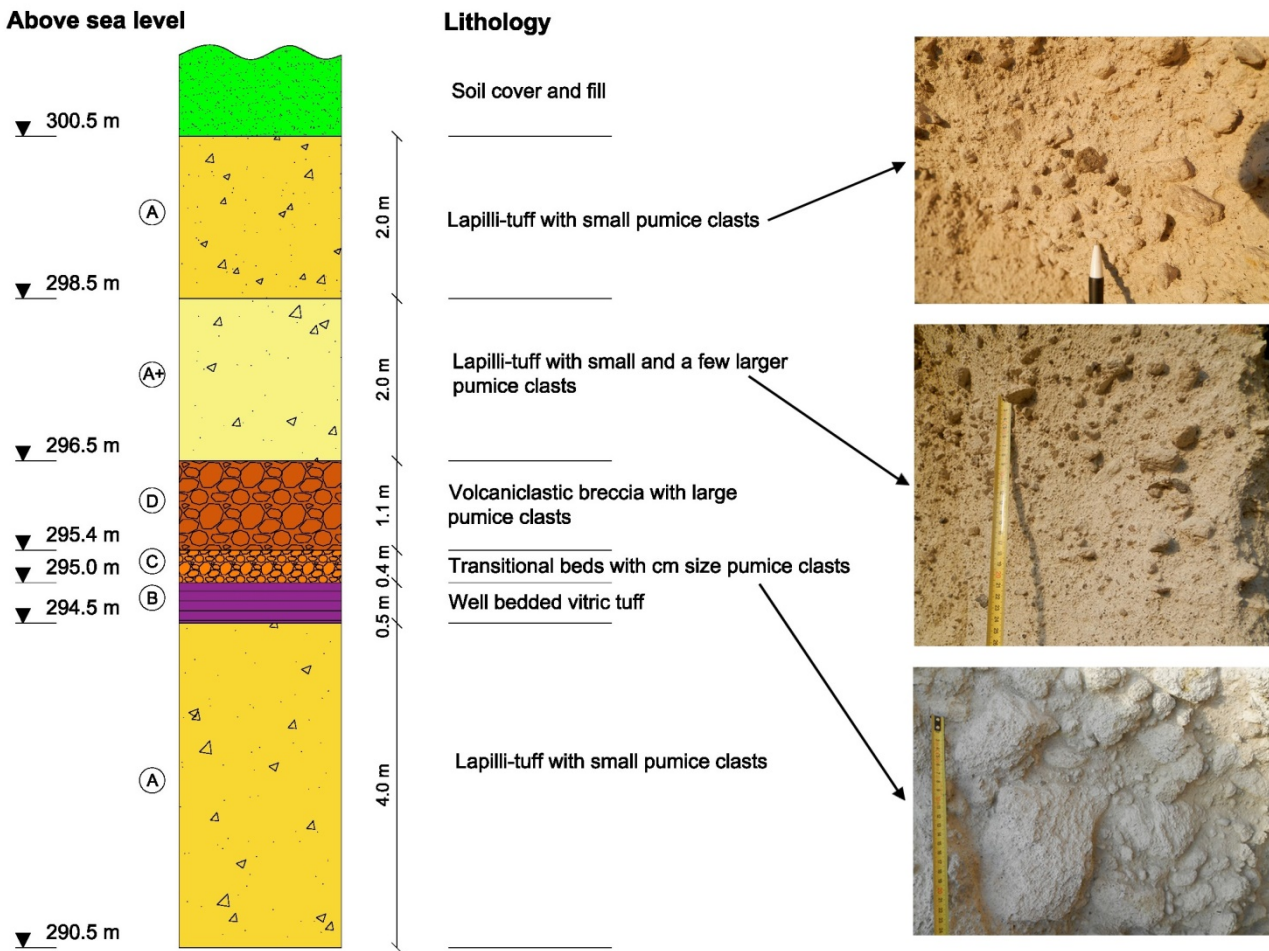
Fig.6. Lithologic column of Sirok Várhegy showing the modelled topmost 10 metres section of the hill (letters refer to lithologic units)

Combining and comparing all measured data of discontinuities and joints, using DTM and morphological index (Fig. 4) the structural geological conditions were clarified: six main joint sets (85/156, 88/312, 79/110, 81/089, 82/064, 61/299) were identified with prevailing NE – SW direction (Fig. 7).
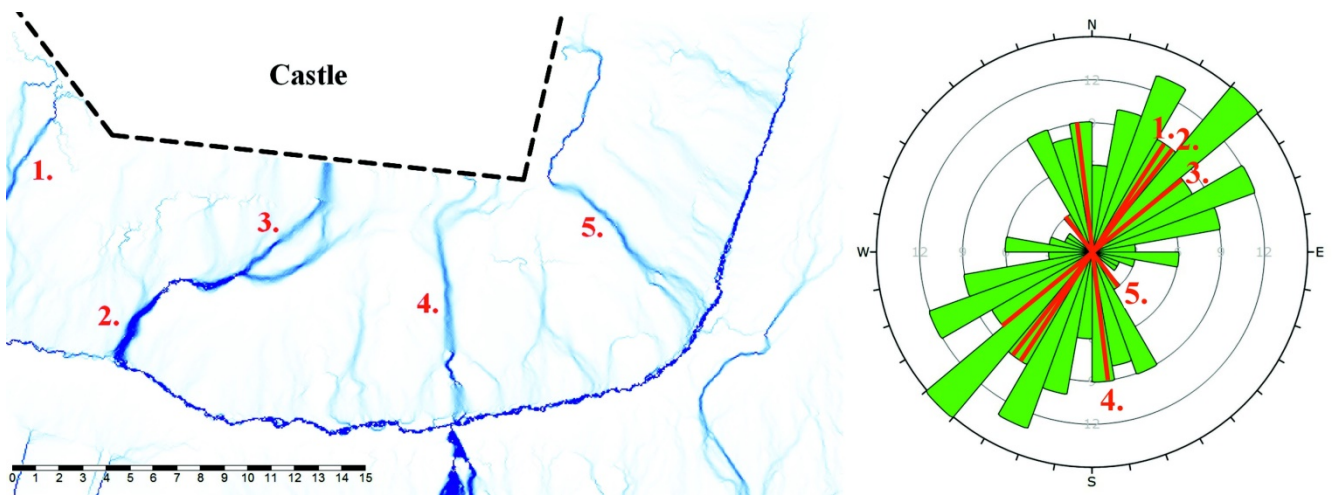
Fig.7. Top view of the cliff (see the location on Fig. 3) obtained with RPAS and the catchment area diagram obtained from DEM analysis (Fig. 4) that was used for joint pattern recognition. Numbers refer to major joint systems marked on DEM map and on
10 **rose diagram of the field measurements and RPAS data set.**

The laboratory tests of tuffs provided the input data for stability analysis for the two main lithologies: upper and lower unit of lapilli tuff and middle unit of less welded tuff (Table 2). In the model calculations GSI=50 value was used.

Table 2. Rock mechanical parameters of tuff used in the model: lapilli tuff refers to upper and lower 4 metres, less welded tuff refers to middle stratigraphic unit

Mechanical property		Upper and Lower unit (marked by A on Fig. 10) (Lapilli tuff)	Middle unit (marked by B-D on Fig. 10) (Less welded tuff)
Bulk density(ρ)	[kg/m³]	1815	1635
Uniaxial compressive strength(σ_c)	[MPa]	8.02	0.35
Tensile strength (σ_t)	[MPa]	0.83	0.04
Modulus of elasticity(E)	[GPa]	0.97	0.05

The results of RS2 FEM analyses suggest that the global factor of safety is SRF=1.27-1.71 in the studied sections (see some of the selected sections are shown on Fig 4). The SRF factor is influenced by the weak tuff layer (Fig. 6) which has very low shear strength compared to the lapilli tuff. Our failure analyses have demonstrated that the bottom of the slip surface would be in the weaker layer (marked by B-D on Fig. 8) and could lead to a larger mass movement.
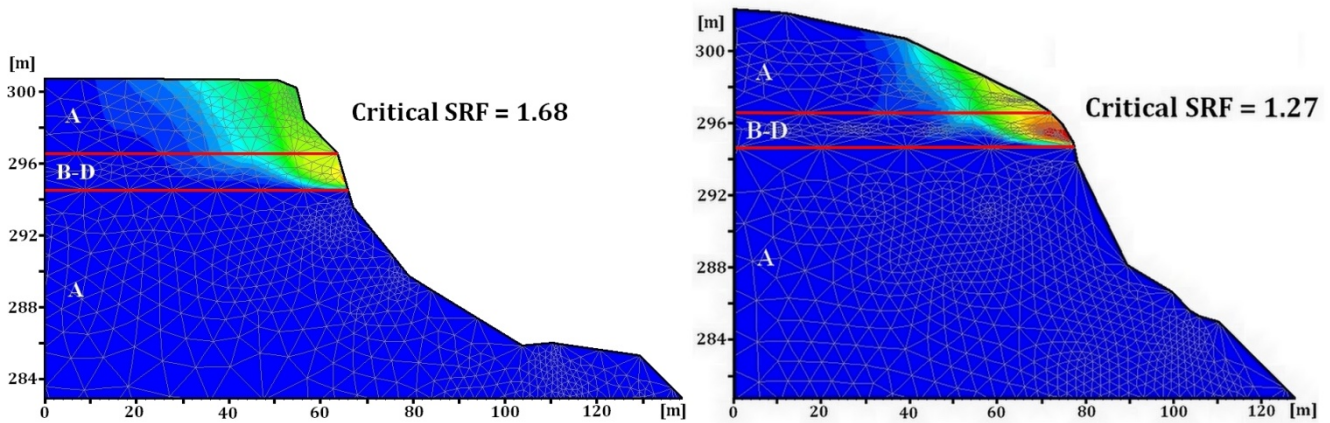
Fig.8. The results of the global stability analysis of the slopes (sections 3 and 4 on Fig. 3), total displacements are marked in blue to red (lithology is indicated by letters A-D, note the weak zone marked by B-D, description of lithologies is given on Fig.6.)

Other failure modes that were studied are planar failure and wedge failure, which are often controlled by joints and discontinuities. According to DTM joint analyses (Fig. 7) and field recordings there was no regular spacing of the discontinuities. Stereographic plots with possible failure planes for all slope directions (Fig. 9) indicate that the most hazardous part of the slope is the one where the plane orientation is 75/75. The calculated factor of safety (FS= 1.15) implies high probability of planar failure.
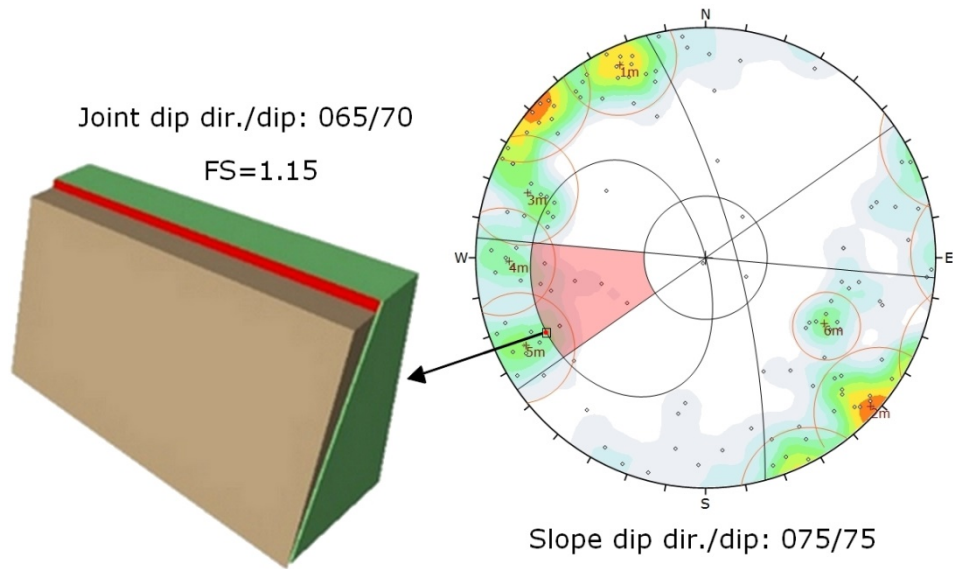
Fig.9. Kinematic analysis of planar failure by Rockplane

Three possible wedge failure modes were identified as being the most hazardous, according to our calculations by Swedge
software (Fig. 10). In these three cases the factor of safety was in the range of 1.38-1.94 representing the hazards of rock
falls along wedges delineated by different joint systems.
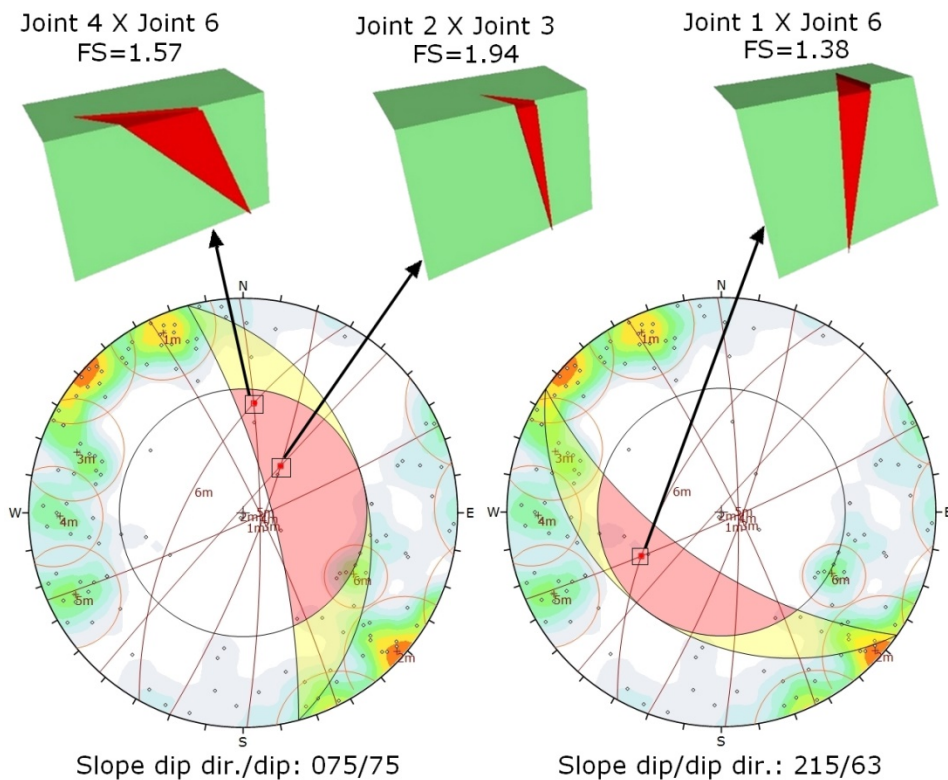
Fig.10. Examples for the kinematic analysis of wedge failures

5. Discussion

There are three critical sets of input data in modelling of rocky slopes: i) terrain model and slope geometry, ii) joints system and iii) strength of rock mass.

To obtain the first, the slope geometry, RPAS based surveying technique was used, because even the hardly accessible cliffs could be surveyed with this method (Giordan et al. 2015). RPAS based data had to be validated. TLS measurements were used for this, in a way that the two point clouds covering the surface were resampled, in order to homogenize the spatial resolution. The point densities have been tested in CloudCompare, as a unit sphere of volume of 1 m3 was defined where the points can be counted and then the sphere can be moved along the whole surface. This computation proved that the average point density in both point clouds are practically the same, although the RPAS densities are more homogeneous, while the TLS has denser point clouds close to the scanning stations.

Another aspect causing some differences between the two data sets is that the image based reconstruction is performed by interest operators, very usually SIFT (Scale-invariant Feature Transform) or similar computer vision operators (Lowe 2004). These operators are generally sensitive to intensity jumps, points, or corners, and textural changes in the input images. If the image resolution is not adequate or the object is locally "smooth", these operators do not return with surface points and the output of the reconstruction has some "filtered" effect. Fortunately, the surface reconstruction quality in RPAS processing resulted minor, ignorable smoothing effect. Comparing the two data sets, it is clearly proven that the geometric resolution of the RPAS-based digital elevation model corresponds to the TLS one, offering the same quality level as the terrestrial laser scanning.

The documentation of joint system and discontinuity surfaces based on field survey provided reliable data on joint orientation; however, the joint system that was found on inaccessible cliffs was not detectable. To overcome this problem, RPAS generated images were used; the frequency of joints was observed based on these images like in previous studies by Assali et al. (2014), Martino & Mazzanti (2014) and Margottini et al. (2015). The required resolution for joint frequency is in the order of 10 cm, rarely 1 cm. The RPAS technique allows having plane surface geometries, however many joints are not plane surfaces and there are hardly visible sets in shadows. Thus RPAS can be used to outline the strike of major joints, but it might causes problem when it comes to the determination of dip and the displacement along the fault planes (e.g. slickensides).

For the determination of the strength of rock masses, we first used Schmidt hammer on site, which is a common practice (Margottini et al. 2015). Our field tests indicate that the application of Schmidt hammer in rock strength analysis is limited when it comes to the analysis of low strength rocks, such as volcanic tuff (Aydan & Ulusay 2003). As a consequence, laboratory analyses of samples were also required to obtain reliable strength parameters. To measure the strength and to understand the weathering characteristics, samples were taken representing different stratigraphic positions. Our lab test data (Table 2) clearly indicates that a low strength unit is found in the studied sections (unit marked by 'B-D' on Fig 8). Whether the low strength of this zone is related to differential weathering or it is associated with inherited weakness (micro-fabric) is not clear. Our results are in good correlations with the previous findings since this volcanic tuff was proved to be very prone to weathering. A loss in tensile strength of 60% was measured under simulated laboratory conditions (Stück et al. 2008). Weathering processes have been long known to induce landslides and cause slope stability problems in various lithologies and especially pyroclastic rocks (Chigra 2002, Fanti et al. 2013). At the studied rhyolite tuff cliff face it was shown that joint system is responsible for slope instabilities: planar and wedge failures were found (Fig. 9., Fig. 10). It is in agreement in several previous works, where the structural geological control of slope stability of highly dissected cliffs was pointed out (Agliardi et al. 2013, Fanti et al. 2013, Feng et al. 2014).

Comparison of surveying techniques obtaining of slope geometry and terrain model data for slope stability analysis helps to choose the appropriate technique (Table 3).

The professional routine is mostly required for classical tachymetry, where the surveyors need to have geological knowledge and surveying expertise to collect the most relevant points. This technology operates usually by the lowest number of measured points, so their quality and distribution is therefore very crucial. The TLS of nowadays are in counterpart very fast instruments (Assali et al. 2014, Neugrig et al. 2016) capturing high amount of terrain points with the ease like using smart phones. Image capture by RPAS is fairly easy; time dependent automatic image capture (e.g. shoot in every second) allows to obtain reliable data. These cameras are mostly equipped by automatic exposure control, which are similar to pocket camera use. One of the drawbacks is that flying requires expertise in flight planning and/or manual operator control. Thanks to onboard electronics, the fastest data capturing method is the RPAS-based. This feature is advantageous if the object availability is limited or the objects are moving/changing. Surveying is the slowest solution to acquire the points, but the data processing is similarly fast (Table 3). TLS and RPAS collected data oblige more processing time – sometimes it is computational hardware dependent. The most homogenous data is obtained by the RPAS methodology; tachymetry can be applied also in this manner, although the efficiency is then very poor (Table 3). TLS has a typical circular pattern having decreasing point density. By corresponding resampling and/or interpolation this drawback can be eliminated. The highest spatial resolution can be achieved by TLS (Table 3). The spatial resolution of RPAS depends on flying time and object distance. Tachymetry is generally a low resolution data collection way. Because tachymeters and laser scanners must stand on the terrain, these technologies are highly dependent from terrain accessibility (slope steepness, vegetation), which is very advantageous for RPAS-based technology (Table 3). RPAS is similarly very robust on shadowing effects, caused by vegetation or other objects. The cost estimations for the given technologies were compiled by the experience taken from the literature. Excellent comparisons and evaluations can be found in Eisenbeiss & Zhang 2006, Koma et al. 2014, Milenkovic et al 2016, Naumann et al. 2013, Rothmund et al. 2013. The data set suggests that on average the costs of RPAS survey are lower than that of TLDS and tachmietry (Table 3).

Table 3. Comparison of the applicability of RPAS-based technology with terrestrial laser scanning (TLS) and tachymetry for rock slope stability assessment. Time frames and applicability is marked by '+' while costs are shown by '$'

	RPAS	TLS	Tachymetry
Required expertise	++	+	+++
Data capturing speed on site (number of obtained data points)	+++	++	+
Required data processing time	++	++	+
Homogeneity of collected data	+++	++	+/++/+++
Resolution	++	+++	+
Difficulty caused by slope accessibility	+	++	++
Digital terrain modelling	+++	+++	+
Slope geometry	+++	+++	++
Joint system detection	+++	+++/++	+
Costs of surveying	$	$$	$$$
Costs of data processing	$$	$$	$

+ low, ++ medium, +++ high, $ low, $$ medium, $$$ high

6. Conclusions

- The use of RPAS technique can overcome the bottleneck of detecting the geometries of highly dissected and inaccessible slopes. RPAS equipped with camera provides relevant amount and quality of imagery data on steep cliff faces.

- Comparing with TLS and tachimetry RPAS technique is much safer; cheaper, faster and provides excellent terrain model after data processing.

- Documentation of joints is essential for cliff face stability analysis. RPAS allows the detection of joint system (mainly strikes and partly dips but not slickensides) but field validation and field measurements of accessible joints and faults are recommended to justify joint orientation obtained from RPAS data based terrain models.

- The lithology and physical parameters of the studied steep cliffs are not uniform and intercalations of weak layers of vitric tuff and volcanoclastic breccia were found.

- According to 2D FEM modelling the intercalating low strength layer is the one where potential slip surface can develop causing larger scale mass movements, but at present it has low probability.

- Joint system has a crucial role in the stability of the studied rhyolite tuff cliff faces. The highest hazard is related to planar failure along ENE-WSW joints and to wedge failure.

Acknowledgements

The help of B. Czinder, B. Kleb, Z. Koppányi, B. Molnár, B. Pálinkás and B. Vásárhelyi is acknowledged. The support of the National Research Development and Innovation (NKFI) Fund (ref. no. K 116532) is appreciated.

References

Abbruzzese, J. M., Sauthier, C., Labiouse, V.: Considerations on Swiss methodologies for rock fall hazard mapping based on trajectory modeling. Nat. Hazards Earth Syst. Sci., 9, 1095–1109, doi:10.5194/nhess-9-1095-2009, 2009.

Agliardi, F., Crosta, G.B., Meloni, F., Valle, C., and Rivolta, C.: Structurally-controlled instability, damage and slope failure in a porphyry rock mass, Tectonophysics 605 (2013) 34–47, doi:10.1016/j.tecto.2013.05.033, 2013.

Arikan, F., Ulusay, R. and Aydin, N.: Characterization of weathered acidic volcanic rocks and a weathering classification based on a rating system. Bulletin of Engineering Geology and the Environment, 66 (4): 415-430, 2007. doi:10.1007/s10064-007-0087-0, 2007.

Assali, P., Grussenmeyer, P., Villemin, T., Pollet, N. and Viguier, F.: Surveying and modelling of rock discontinuities by terrestrial laser scanning and photogrammetry: Semi-automatic approaches for linear outcrop inspection. J. of Struct. Geol., 66: 102-114, doi:10.1016/j.jsg.2014.05.014, 2014.

Aydan, Ö., and Ulusay, R.: Geotechnical and environmental characteristics of man-made underground structures in Cappadocia, Turkey. Eng. Geol., 69 (3/4): 245-272, doi:10.1016/S0013-7952(02)00285-5, 2003.

Balogh K.: Geological Formations of Bükk Mountains (in Hungarian), Annual Report of the Hungarian Geological Survey, 48(2), 245-719 1964.

Brauneck, J., Pohl, R., Juepner, R.: Experiences of using UAVs for monitoring levee breaches. IOP Conf. Series: Earth and Environmental Science 46, 012046, IOP Publishing, doi:10.1088/1755-1315/46/1/012046, 2016.

Budetta, P.: Assessment of rockfall risk along roads, Nat. Hazards Earth Syst. Sci., 4, 71–81, doi:10.5194/nhess-4-71-2004, 2004.

Casella, E., Rovere, A., Pedroncini, A., Stark, C. P., Casella, M., Ferrari, M., Firpo, M.: Drones as tools for monitoring beach topography changes in the Ligurian Sea (NW Mediterranean), Geo-Marine Letters, 36(2), 151-163., doi:10.1007/s00367-016-0435-9, 2016.

Chigira, M.: Geologic factors contributing to landslide generation in a pyroclastic area: August 1998 Nishigo Village, Japan, Geomorphology, Vol. 46(1-2), 117-128, doi:10.1016/S0169-555X(02)00058-2, 2002.

Cloud Compare point cloud processing software (CC) available at: http://www.cloudcompare.org/ (last access 1 February 2017), 2014

Conrad, O., Bechtel, B., Bock, M., Dietrich, H., Fischer, E., Gerlitz, L., Wehberg, J., Wichmann, V., and Böhner, J.: System for Automated Geoscientific Analyses (SAGA) v. 2.1.4, Geosci. Model Dev., 8, 1991-2007, doi:10.5194/gmd-8-1991-2015, 2015.

Copons, R., Vilaplana, J. M., and Linares, R.: Rockfall travel distance analysis by using empirical models (Solà d'Andorra la Vella, Central Pyrenees), Nat. Hazards Earth Syst. Sci., 9, 2107-2118, doi:10.5194/nhess-9-2107-2009, 2009.

Crosta, G, and Agliardi, F.: How to obtain alert velocity thresholds for large rockslides. Phys Chem Earth Parts ABC. 27:1557-1565, doi:10.1016/S1474-7065(02)00177-8, 2002.

Crosta, G. B., and Agliardi, F.: A methodology for physically based rockfall hazard assessment. Natural Hazards and Earth System Sciences 3: 407–422, doi:10.5194/nhess-3-407-2003, 2003.

Danzi M., Di Crescenzo G., Ramondini M., Santo A. Use of unmanned aerial vehicles (UAVs) for photogrammetric surveys in rockfall instability studies, Rend. Online Soc. Geol. It., Vol. XX, doi: 10.3301/Rol.2012.xx, 2013.

De Biagi, V., Napoli, M.L., Barbero, M., and Peila, D.: Estimation of the return period of rockfall blocks according to their size. Nat. Hazards Earth Syst. Sci., 17, 103–113, 2017, doi:10.5194/nhess-17-103-2017, 2017.

DJI phantom 2 quadrocopter (DJI) available at: http://www.dji.com/phantom-2 (last access 1 February 2017), 2015.

Eisenbeiss, H., Zhang, L. (2006): Comparison of DSMs generated from mini UAV imagery and terrestrial laser scanner in a cultural heritage application, International Archives of the Photogrammetry, Remote Sensing and Spatial Information Sciences, Volume XXXV/5, pp. 90-96

Fanti, R., Gigli, G., Lombardi, L., Tapete, D., Canuti, P., Terrestrial laser scanning for rockfall stability analysis in the cultural heritage site of Pitigliano (Italy). Landslides 10:409–420, DOI 10.1007/s10346-012-0329-5, 2013.

Faro terrestrial laser scanner (Faro) available at: http://www.faro.com/en-us/products/3d-surveying/faro-focus3d/overview (last access 1 February 2017), 2016.

Feng, Z., Li, B., Yin, Y. P., and He, K.: Rockslides on limestone cliffs with subhorizontal bedding in the southwestern calcareous area of China. Nat. Hazards Earth Syst. Sci., 14, 2627-2635, doi:10.5194/nhess-14-2627-2014, 2014.

Francioni, M., Salvini, R., Stead, D., and Litrico, S.: A case study integrating remote sensing and distinct element analysis to quarry slope stability assessment in the Monte Altissimo area, Italy. Eng. Geol., 183: 290-302., doi:10.1016/j.enggeo.2014.09.003, 2014.

Fraštia, M., Marčiš, M., Kopecký, M., Liščák, P., Žilka, A.: Complex geodetic and photogrammetric monitoring of the Kraľovany rock slide. Journal of Sustainable Mining, 13(4), 12–16. doi: 10.7424/jsm140403, 2014.

Geomagic Design X 3D modelling software (GeomagicDesignX) available at: http://www.geomagic.com/en/products-landing-pages/designx (last access 1 February 2017), 2016

Geomagic Studio 3D modelling software (GeomagicStudio) available at: http://www.geomagic.com/en/ (last access 1 February 2017), 2013

Giordan, D., Manconi A., Allasia P., and Bertolo D.: Brief Communication: On the rapid and efficient monitoring results dissemination in landslide emergency scenarios: the Mont de La Saxe case study. Nat. Hazards Earth Syst. Sci., 15, 2009–2017, 2015, oi:10.5194/nhess-15-2009-2015, 2015.

GoPro action cam (GoPro) available at: https://gopro.com/ (last access 1 February 2017), 2017

Haas, F., Hilger, L., Neugirg, F., Umstädter, K., Breitung, C., Fischer, P., Hilger, P., Heckmann, T., Dusik, J., Kaiser, A., Schmidt, J., Della Seta, M., Rosenkranz, R., and Becht, M.: Quantification and analysis of geomorphic processes on a recultivated iron ore mine on the Italian island of Elba using long-term ground-based lidar and photogrammetric SfM data by a UAV, Nat. Hazards Earth Syst. Sci., 16, 1269-1288, doi:10.5194/nhess-16-1269-2016, 2016.

Hoek, E., Carranza-Torres, C., and Corkum, B.: Hoek-Brown failure criterion – 2002 Edition. Proc. NARMS-TAC Conference, Toronto, 1, 267-273, 2002.

Inverse distance weighting interpolation (IDW) available at: http://gisgeography.com/inverse-distance-weighting-idw-interpolation/ (last access 1 February 2017), 2013

5 Jovančević, S. D., Peranić, J., Ružić, I. and Arbanas, Ž.: Analysis of a historical landslide in the Rječina River Valley, Croatia. Geoenvironmental Disasters, 3:26, doi:10.1186/s40677-016-0061-x, 2016.

Koma, Zs., Székely, B., Dorninger, P., Rasztovits, S., Roncat, A., Zámolyi, A., Krawczyk, D., Pfeifer, N. (2014): Comparison of UAV and TLS DTMs for acquisition of geological, geomorphological information for Doren landslide, Vorarlberg Austria, EGU General Assembly Conference Abstracts, 2014

10 LAS laser scanner point cloud datatype specification (LAS) available at: https://www.asprs.org/committee-general/laser-las-file-format-exchange-activities.html (last access 1 February 2017), 2012

Leica CS10 controller (CS10) available at: http://leica-geosystems.com/products/gnss-systems/controllers/leica-viva-cs15-and-cs10 (last access 1 February 2017), 2014

Leica Cyclone point cloud processing software (LeicaCyclone) available at: http://leica-geosystems.com/products/laser-scanners/software/leica-cyclone (last access 1 February 2017), 2016

Leica GNSS receiver (GS08) available at: http://leica-geosystems.com/products/gnss-systems/smart-antennas/leica-viva-gs08plus (last access 1 February 2017), 2014

Lowe, D.G. (2004): International Journal of Computer Vision 60: 91, doi: 10.1023/B:VISI.0000029664.99615.94

Manconi, A., and Giordan, D.: Landslide failure forecast in near-real-time, Geomatics, Natural Hazards and Risk, 2014, doi:10.1080/19475705.2014.942388, 2014.

20

Manconi, A., and Giordan, D.: Landslide early warning based on failure forecast models: the example of the Mt. de La Saxe rockslide, northern Italy. Nat. Hazards Earth Syst. Sci., 15, 1639–1644, 2015, doi:10.5194/nhess-15-1639-2015, 2015.

Margottini, C., Antidze, N., Corominas, J., Crosta, G.B., Frattini, P., Gigli, G., Giordan, D., Iwasaky, I., Lollino, G., Manconi, A., Marinos, P., Scavia, C., Sonnessa, A., Spizzichino, D., and Vacheishvili, N.: Landslide hazard, monitoring and conservation strategy for the safeguard of Vardzia Byzantine monastery complex, Georgia. Landslides 12:193–204, doi:10.1007/s10346-014-0548-z, 2015.

25

Marinos, V., Marinos, P., and Hoek, E.: The geological strength index: applications and limitations. Bull Eng Geol Environ 64: 55–65, doi:10.1007/s10064-004-0270-5, 2005.

Martino, S., and Mazzanti, P.: Integrating geomechanical surveys and remote sensing for sea cliff slope stability analysis: the Mt. Pucci case study (Italy). Nat. Hazards Earth Syst. Sci., 14, 831-848, doi:10.5194/nhess-14-831-2014, 2014.

30

Mateos, R.M., García-Moreno, I., Reichenbach, P., Herrera, G., Sarro, R., Rius, J., Aguiló, R., and Fiorucci, F.: Calibration and validation of rockfall modeling at regional scale: application along a roadway in Mallorca (Spain) and organization of its management. Landslides 13:751–763, doi:10.1007/s10346-015-0602-5, 2016.

Mathworks Matlab mathematical environment (Matlab) available at: https://www.mathworks.com/products/matlab.html, (last access 1 February 2017), 2017

35

Michoud, C., Derron, M.-H., Horton, P., Jaboyedoff, M., Baillifard, F.-J., Loye, A., Nicolet, P., Pedrazzini, A., and Queyrel, A.: Rockfall hazard and risk assessments along roads at a regional scale: example in Swiss Alps. Nat. Hazards Earth Syst. Sci., 12, 615–629, 2012. doi:10.5194/nhess-12-615-2012, 2012.

Milenkovic, M.,Karel, W., Ressl, C., Pfeifer, N.: A comparison of UAV and TLS data for soil roughness assessment, ISPRS Annals of the Photogrammetry, Remote Sensing and Spatial Information Sciences, Volume III-5, pp. 145-152, doi:10.5194/isprsannals-III-5-145-2016, 2016.

40

Naumann, M., Geist, M., Bill, R., Niemeyer, F., Grenzdörffer, G.: Accuracy comparison of digital surface models created by unmanned aerial systems imagery and terrestrial laser scanner, International Archives of the Photogrammetry, Remote Sensing and Spatial Information Sciences, Volume XL-1/W2, pp. 281-286, 2013.

Neugirg, F. Stark, M. Kaiser A., Vlacilova M., Della Seta M., Vergari F., Schmidt J.,. Becht M, Haas F. Erosion processes in calanchi in the Upper Orcia Valley, Southern Tuscany, Italy based on multitemporal high-resolution terrestrial LiDAR and UAV surveys. Geomorphology, 269, 8-22. doi: 10.1016/j.geomorph.2016.06.027, 2016.

Niethammer, U., James, M.R., Rothmund, S., Travelletti, J., Joswig, M. UAV-based remote sensing of the Super-Sauze landslide: Evaluation and results. Engineering Geology 128, 2-11, doi: 10.1016/j.enggeo.2011.03.012, 2012.

Pappalardo, G., Mineo, S., and Rapisarda, F.: Rockfall hazard assessment along a road on the Peloritani Mountains (northeastern Sicily, Italy) Nat. Hazards Earth Syst. Sci., 14, 2735-2748, doi:10.5194/nhess-14-2735-2014, 2014.

Pix4D photogrammetry software (Pix4D) available at: https://pix4d.com/product/pix4dmapper-pro/ (last access 1 February 2017), 2017

Rau, J., Jhan, J., Lob, C., Linb, Y. Landslide mapping using imagery acquired by a fixed-wing UAV. ISPRS – Int. Arch. Photogramm. Remote Sens. Spatial Inform. Sci. XXXVIII-1/C22, 195–200, 2011.

Real time kinematic net service (RTKnet) available at: https://www.gnssnet.hu (last access 1 February 2017), 2013

Rothmund, S., Niethammer, U., Walter, M., Joswig, M.: Comparison of DSMs acquired by terrestrial laser scanning, UAV-based aerial images and ground-based optical images at the Super-Sauze landslide, EGU General Assembly Conference Abstracts, 2013.

Samodra, G., Chen, G., Sartohadi, J., Hadmoko, D.S., Kasama, K., and Setiawan, M.A.: Rockfall susceptibility zoning based on back analysis of rockfall deposit inventory in Gunung Kelir, Java. Landslides (2016) 13:805–819, doi:10.1007/s10346-016-0713-7., 2016.

Stead, D. Wolter A. A critical review of rock slope failure mechanisms: The importance of structural geology. J. Structural Geology, 74, 1-23. doi: 10.1016/j.jsg.2015.02.002, 2015.

Stück, H., Forgó, L.Z., Rüdrich, J., Siegesmund, S., Török, Á.: The behaviour of consolidated volcanic tuffs: weathering mechanisms under simulated laboratory conditions, Environmental Geology, Vol. 56(3-4), 699-713, doi:10.1007/s00254-008-1337-6, 2008.

Török, Á., Forgó, L.Z. Vogt, T., Löbens, S., Siegesmund, S., and Weiss, T.: The influence of lithology and pore-size distribution on the durability of acid volcanic tuffs, Hungary. Prykril, R. & Smith, J.B. (Eds.): Building Stone Decay: From Diagnosis to Conservation, Geological Society, London, Special Publications 271: 251-260, 2007.

Westoby M.J., Brasington J., Glasser N.F., Hambrey M.J., Reynolds J.M. Structure-from-Motion' photogrammetry: A low-cost, effective tool for geoscience applications, Geomorphology, Volume 179, Elsevier, pp. 300–314, doi: 10.1016/j.geomorph.2012.08.021, 2012.

Z+F terrestrial laser scanner (Z+F) available at: http://www.zf-laser.com/Z-F-IMAGER-R-5010C.3d_laserscanner.0.html?&L=1 (last access 1 February 2017), 2014.